



OPEN

SUBJECT AREAS:

ENVIRONMENTAL

MONITORING

PHYSICAL OCEANOGRAPHY

Received 22 April 2014 Accepted 16 July 2014 Published 4 August 2014

Correspondence and requests for materials should be addressed to Z.F.L. (Izhifei@tongji. edu.cn)

Mesoscale eddies transport deep-sea sediments

Yanwei Zhang¹, Zhifei Liu¹, Yulong Zhao¹, Wenguang Wang¹, Jianru Li¹ & Jingping Xu²

¹ State Key Laboratory of Marine Geology, Tongji University, Shanghai 200092, China, ²U.S. Geological Survey, Santa Cruz, CA 95060, USA.

Mesoscale eddies, which contribute to long-distance water mass transport and biogeochemical budget in the upper ocean, have recently been taken into assessment of the deep-sea hydrodynamic variability. However, how such eddies influence sediment movement in the deepwater environment has not been explored. Here for the first time we observed deep-sea sediment transport processes driven by mesoscale eddies in the northern South China Sea via a full-water column mooring system located at 2100 m water depth. Two southwestward propagating, deep-reaching anticyclonic eddies passed by the study site during January to March 2012 and November 2012 to January 2013, respectively. Our multiple moored instruments recorded simultaneous or lagging enhancement of suspended sediment concentration with full-water column velocity and temperature anomalies. We interpret these suspended sediments to have been trapped and transported from the southwest of Taiwan by the mesoscale eddies. The net near-bottom southwestward sediment transport by the two events is estimated up to one million tons. Our study highlights the significance of surface-generated mesoscale eddies on the deepwater sedimentary dynamic process.

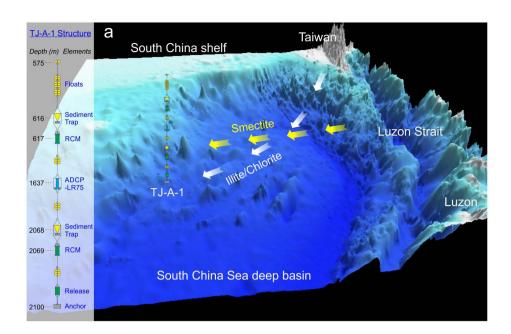
urface mesoscale eddies have been proved to be substantial in investigating fluxes of water mass, energy, heat, nutrients, and other biogeochemical properties in the upper ocean¹⁻⁶. Due to the high nonlinearity of westward propagating eddy, water can be trapped inside the eddy without dispersion and transported for a long distance⁷. Recent results from *in situ* observations demonstrate an unexpected influence of surface-generated mesoscale eddies in the transport of hydrothermal vent efflux away from the deep East Pacific Rise⁸, suggesting that these deep-reaching eddies could have a great impact on deep-sea sediment transport⁹.

As an active and ideal region for generation and propagation of mesoscale eddies, the South China Sea (SCS) has been investigated through both observation and numerical modelling for kinematic mechanism and hydrographic structure of these mesoscale eddies^{10–12}. However, how such eddies influence the deep-sea sediment dynamic process has not been explored yet. For this purpose, we deployed a full-water column mooring system (TJ-A-1) equipped with Acoustic Doppler Current Profiler (ADCP), Recording Current Meter (RCM), and sediment trap systems at the lower continental slope with a water depth of 2100 m in the northeastern SCS (Figure 1a). The observed current velocity, temperature, and suspended sediment concentration (SSC) data, spanning nearly two years (from September 2011 to May 2013), reveal two southwestward deepwater sediment transport events that are attributed to the identified surface mesoscale eddy activities. Our study is for the first time to have observed how the upper-ocean hydrodynamic process affects the cross-basin sediment transport in the deepwater environment.

Results

Co-variation in deepwater current oscillation and sea-surface eddy occurrence. High-resolution sea surface level anomaly (SLA) fields produced through merging measurements from four simultaneously operating satellites reveal that two anticyclonic eddies (with positive SLA) with radii of ~150 km crossed the mooring site from January to March 2012 and from November 2012 to January 2013, respectively (Figure 1b). Besides, a cyclonic eddy (with negative SLA) was accompanied with the first anticyclonic eddy in March 2012 with limited influence on the mooring site. Both anticyclonic eddies originated in the southwest of Taiwan and propagated southwestward with a speed averaging at 10 cm s⁻¹. The first anticyclonic eddy crossed the mooring site from 26 January to 8 March 2012 (Supplementary Movie S1), and the second one passed by from 26 November 2012 to 10 January 2013 (Supplementary Movie S2). The immediate or lagging changes in current velocity and direction observed from surface through near-bottom (Figure 2, Supplementary Figure S1) are consistent with the interference of hydrodynamic processes resulted from the surface eddies. The amplitude of current velocities at all depths were almost twice the normal values when the two anticyclonic eddies passed through.





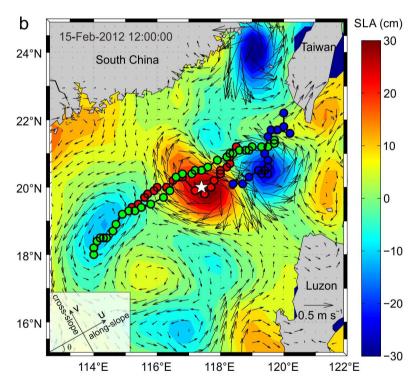


Figure 1 | Seafloor topography and sea surface level anomaly in the northeastern South China Sea (SCS). (a) Seafloor topography showing the location of the TJ-A-1 mooring system and its vertical structure (left side). The three-dimensional topography map is created from the 30-arc-second resolution global topography/bathymetry grid (STRM30_PLUS)¹³ using Global Mapper 12. Two RCMs are equipped with probes for turbidity and temperature measurement (see Methods for more details of the mooring system). Potential sediment transport pathways of illite and chlorite derived from Taiwan and smectite originated from Luzon are also displayed¹⁴. (b) Map of sea level anomaly (SLA) with surface geostrophic current velocity (shown as black arrows) on 15 February 2012 when an anticyclonic eddy passed by the mooring site (white star). The map is generated through combining SLA and surface geostrophic current velocity data distributed by AVISO (http://www.aviso.oceanobs.com) using Matlab R2010b. Centroidal tracks of three eddies from birth until death, marked every 3 days (circles), are superimposed on the map. Red and blue circles stand for an anticyclonic and a cyclonic eddy born in November 2011, respectively; green circles represent an anticyclonic eddy born in November 2012. The inset figure in the lower part of (b) shows the u (along-slope) and v (cross-slope) coordinates (see Methods for detailed descriptions).

Correspondingly, the main direction of current velocity shifted from northwestward to southeastward, following a clockwise rotation of the anticyclonic eddies. Besides the associated change in current velocities, the downward water temperatures also display a distinct

decrease when both mesoscale eddies passed through (Supplementary Figures S2 and S3).

The cross-correlation between the surface geostrophic velocities and observed current velocities and SSC at different depths further



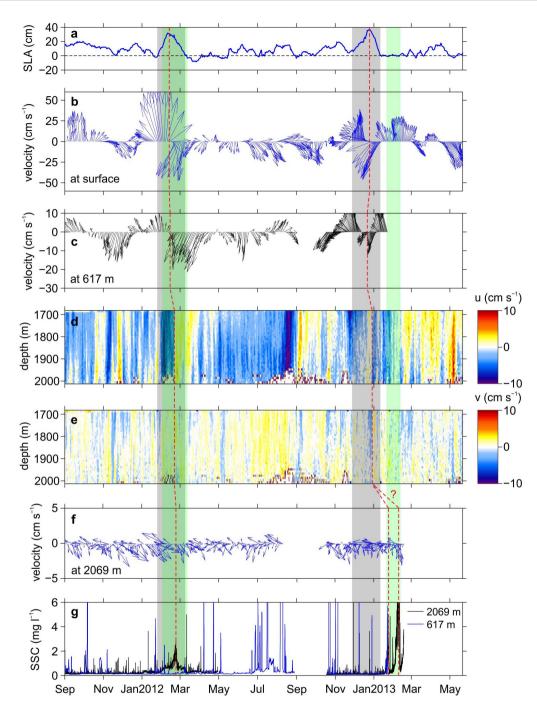


Figure 2 | Time series of SLA, current velocity, and suspended sediment concentration (SSC) variations from September 2011 to May 2013. Shaded regions show the periods when two energetic anticyclonic eddies passed through the mooring site (gray) and the periods with enhanced SSC near the seafloor (green) following the eddy activities. Red dashed lines indicate the influence of the anticyclonic eddies through the full water column.

(a) Surface SLA showing two anticyclonic eddies passed through during the observation period: one in January to March 2012 and the other in November 2012 to January 2013. (b) Surface geostrophic velocity derived from the SLA. (c) Current velocity recorded at 617 m water depth by a RCM. (d) Along-slope velocity (u) profile recorded by a down-looking ADCP-LR75 positioned at 1637 m water depth (~460 m above seafloor). (e) Same as (d) but for cross-slope velocity (v) profile. (f) Current velocity recorded at 2069 m water depth by a RCM. (g) The SSC recorded by turbidity probes associated with RCMs positioned at 617 m (blue curve) and 2069 m (black curve) water depths, respectively. A question mark (?) to the red dashed line in the green shaded region shows an uncertainty of correlation. See Figure 1a for details of instrument positions in the mooring system.

indicates a close relationship of the anomalous current velocities with the passing-through anticyclonic eddies (Figure 3). The Pearson correlation coefficients between velocities at the surface and at 617 m (Figure 2b and 2c), at the 95% confidence level for the full record when the two eddies passed through, display a significant correlation ($R_{\rm u}=0.48,\,R_{\rm v}=0.57$ when the first eddy got through; $R_{\rm u}=-0.28,\,R_{\rm v}=0.47$ when the second eddy passed). Due to the similarity of

current velocities recorded at depths by ADCP and RCM (Supplementary Figure S1), we here take the velocity recorded by RCM at 2069 m to represent the near-bottom current velocity in the following analysis. Observed near-bottom current velocity (at 2069 m, Figure 2f) is also significantly correlated with the surface geostrophic current velocity, which is associated with the eddy activities ($R_u=0.47,\,R_v=-0.65$ when the first eddy passed through; $R_u=0.47$, $R_v=0.47$, $R_v=0.65$ when the first eddy passed through; $R_u=0.47$, $R_v=0.47$, $R_v=0.65$ when the first eddy passed through; $R_u=0.47$, $R_v=0.47$,

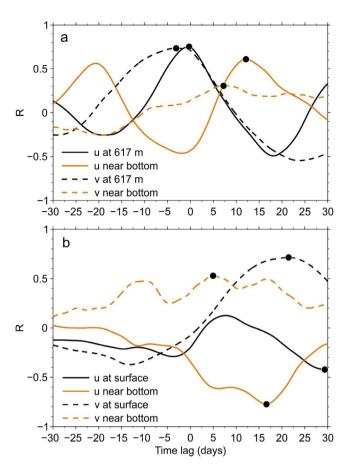


Figure 3 | Lag-correlations between current velocities and SSC during the period when the eddies passing through the mooring site. (a) Lag-correlations between surface geostrophic velocities and current velocities observed at 617 m (black curves) and near-bottom (brown curves). (b) Lag-correlations between the SSC observed near bottom (at 2069 m) and velocities of sea surface (black curves) and near bottom (at 2069 m, brown curves). Solid curves represent along-slope velocities (u), and dashed curves represent cross-slope velocities (v); the maximal correlation coefficients are marked with black dots.

 $=-0.44,\,\mathrm{R_v}=0.12$ when the second eddy passed). P-values for testing the hypothesis of no correlation are also calculated. All the P-values for the Pearson correlation coefficients in this study are less than 0.001 (the duration of the eddy is chosen as the time interval for the lag correlation), indicating a significant correlation. The correlation analysis suggests that eddy-driven impacts extend through the upper ocean into the deep, resulting in potential influences on deepwater dynamics.

Given the potential offset between the surface and deep flows and the different vertical structure of the two anticyclonic eddies, various time lags among velocities at the surface and at depth are found. We take the first eddy as an example to determine the optimal time lag from the maximal correlation coefficients (Figure 3a). About 4 days in advance are distinguished between the surface geostrophic velocity and the observed velocity at 617 m ($R_{\rm u}=0.75,\,R_{\rm v}=0.73$). A longer time lag occurred for the current velocity in the deeper layer. The along-slope velocity near the bottom lagged the along-slope surface geostrophic velocity by 12 days at the maximal correlation ($R_{\rm u}=0.61$). The optimal time lag for the cross-slope velocity near the bottom is 7 days at the maximal correlation ($R_{\rm v}=0.31$). The various optimal time lags for the anomalous velocities at different depths suggest that the influence induced by the passing eddy can result in complicated dynamic responses under the benthic environment.

Such lags and offsets between surface and deep flows in the mesoscale eddies were well simulated for the near bottom transport of hydrothermal vent larvae on the northern East Pacific Rise¹⁵.

Eddy influence on deepwater sediments. Twice dramatic increases in the near-bottom SSC (Figure 2g, black curve) were fully observed by the turbidity probe equipped on a RCM located at 2069 m (31 m above the seafloor) and corresponded to the periods of anomalous current velocities. The influence of eddies is evident from the simultaneous variations in the SLA (Figure 2a) and SSC (Figure 2g) when the mesoscale eddies passed through. The increase in SSC lasts from 1 February to 10 March 2012, when the first anticyclonic eddy passed by the mooring site. The near-bottom SSC is enhanced almost 6 folds to a maximum of 2.8 mg l⁻¹ with a mean value of 1.2 mg l⁻¹, comparing to the background value of 0.2 mg l⁻¹. Two enhanced SSC events occurred when the second anticyclonic eddy came over. The first increase in SSC has the similar mean value of 1.2 mg l⁻¹ with a maximum of 3.1 mg l⁻¹, but with a shorter duration from 19 to 25 January 2013. The mean value of the second enhanced SSC event (from 30 January to 12 February 2013) is up to 2.8 mg l^{-1} with a maximum of 8.5 mg l^{-1} . The different durations of enhanced SSC induced by the two eddies could result from their different vertical structures and pathways across the mooring site (Figure 2d, Supplementary Movies S1 and S2). In early 2012, it is the center of the eddy, while in early 2013 its south margin, passed the mooring site. We suggest a one-month lag of deepwater velocity variation in January 2013 to be strongly related to complicated structure of the second anticyclonic eddy. Being short of observed data on the latter event in 2013 (failure of turbidity probe equipped on the upper RCM), the gap of about one week between the two high values of SSC needs further investigation (a question mark addresses an uncertainty of correlation in Figure 2f).

To investigate the relationship between the enhanced SSC and the hydrodynamic event driven by eddies, the lag-correlations between SSC and anomalous velocities are shown in Figure 3b (also taking the first eddy as an example). Considering the direction changes in the rotational velocity accompanied with the southwestward-propagating eddies (Supplementary Movies S1 and S2), the along-slope (u) and cross-slope (v) velocities potentially have different influence on SSC. The lag of maximal correlations between SSC and near-bottom velocities (brown curves in Figure 3b, with Ru = 0.77 and Rv = 0.53) indicates that the extrema of SSC lags the extrema of eddy-induced anomalous along-slope velocity by 17 days near the bottom. As a result of the lag between the near-bottom and surface velocities, there are longer lags between the observed near-bottom SSC and the surface geostrophic velocities. Specifically, the enhanced SSC lags the surface along-slope velocity by 29 days with a maximal correlation (Ru = -0.42) and 21 days with a maximal correlation (Rv = 0.71) for surface cross-slope velocity, respectively (black curves in Figure 3b). As indicated by the lag correlation in Figure 3b, the eddy-induced hydrodynamic influence on the observed near-bottom SSC lasted longer than one month. These statistics further suggest that the enhanced SSC is associated the eddy-induced anomalous

The distinguishable increases of suspended sediments collected by sediment traps further support the eddy influence on the dramatic increase in southwestward sediment transport (Figure 4). The amount of sediments collected near the bottom (at 2068 m, the position of the lower sediment trap) increased dramatically during the second eddy passed through (Figure 4c), consistent with the nearbottom increase in the SSC (Figure 4d). Despite of the failure of the lower-layer sediment trap operation during the first deployment (September 2011 to October 2012), the occurrence of a similar increase of suspended sediments is assumed through our observation of the near-bottom SSC (Figure 4a) when the first eddy passed by the mooring site during January and February 2012. The results show



that the passing eddies potentially provided a conduit for sediment transport in the deep sea.

New understanding on sediment cross-basin transport in the SCS. Eddies have been shown to transport plumes of suspended sediments and nutrients from continental shelves into the deep ocean^{6,9}. The transport ability is a function of the nonlinearity of eddy^{16,17}, which can be quantified by a nondimentional ratio of maximal surface geostrophic speed (U) to propagation speed (c) of the eddy. As acknowledged from previous studies^{7,17}, when U/c > 1, the feature is nonlinear, and the eddy can effectively trap and transport water properties. The U/c ratio is approximate 5 for the two eddies in this study, indicating a clear nonlinear feature. The southwest of Taiwan where eddies are frequently born is a region that receives huge amount of terrigenous sediments from Taiwan rivers¹⁸. The finegrained sediments mainly in illite and chlorite of clay minerals that derived from Taiwan rivers are considered to be transported to our mooring site through potential deepwater currents^{14,19} (Figure 1a). Our new analysis on the filtrated suspended sediment at ~2000 m water depth (about 68 m above the lower-layer sediment trap) presents a high Taiwan-sourced illite and chlorite terrigenous particles with a total value up to 59 \pm 5% (see Methods for the analysis). Therefore, the southwest of Taiwan acts as the most likely source of the high SSC observed at our mooring site.

On the assumption that the SSC at the origin of the eddies could be similar as they reached our mooring site and taking a width of 100 km and a thickness of 100 m for the high SSC layer near the bottom, we here estimate the sediment mass transported through the along-slope-propagating mesoscale eddies. The sediment transport mainly occurred along-slope with a maximal transport mass of 600 kg s⁻¹ (red curves in Figure 4b and 4e). As indicated in Figure 4b, the southwestward sediment transport (with negative transport values) when the first eddy approached to the study site and the northeastward sediment transport (with positive transport values) when the eddy departed were observed, respectively. During passing through of the first eddy, the total southwestward and northeastward sediment transport mass was up to 6.8×10^8 kg and $1.6 \times$ 108 kg, respectively, resulting in a net southwestward sediment transport mass of about 5.2×10^8 kg. For the second anticyclonic eddy, the along-slope sediment transport mass was 3.9×10^8 kg for the first enhanced SSC event (19 to 25 January 2013, the near-bottom current velocity was continuously southwestward) and 1.4×10^8 kg for the second one (30 January to 12 February 2013, with frequent reversal current velocities resulting in less net sediment transport),

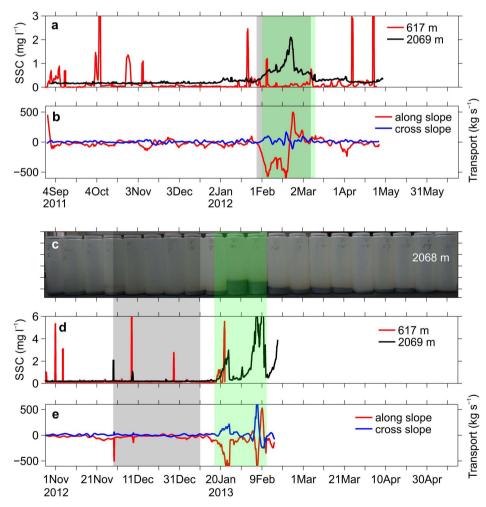


Figure 4 | Time series of suspended sediment responses to passing-through of two anticyclonic eddies. During passing-through of the first eddy: (a) SSC near-bottom (black curve) and upper layer (at 617 m, red curve), same as Figure 2g but with 3-day filtered; (b) sediment transport mass estimated from the SSC shown in (a) and corresponding near-bottom velocities. During passing-through of the second eddy: (c) bottled sediment samples collected by the lower-layer sediment trap positioned at 2068 m (~32 m above the seafloor); (d) SSC near-bottom (black curve) and upper layer (at 617 m, red curve), same as Figure 2g but with 3-day filtered; (e) sediment transport mass estimated from the SSC shown in (d) and corresponding near-bottom velocities. The lower-layer sediment trap during the first deployment (September 2011 to October 2012) failed in the operation, and then no bottled sediment samples are provided when the first eddy passed through. Shaded regions are same as in Figure 2.



respectively. As a result, the total net southwestward sediment transport mass driven by these two mesoscale eddies is about 10.5 \times 108 kg, amounting to \sim 2% of the total annual sediment discharge from western Taiwan rivers²⁰.

Discussion

The SCS receives more than 600 million tons of detrital sediment annually from numerous surrounding rivers, and upon entering the sea, the sediments are further transported by various coastal, surface, and deep/bottom currents21. However, the suspicious stability and even existence of deep current in the SCS although deduced from modelling²² challenges the deepwater sediment transport ability. Our long-term, full-water column observation reveals that surface mesoscale eddies not only penetrate into the deep sea, but also transport sediments in the deepwater environment. Although the observed increase in the SSC when the mesoscale eddies passed through the mooring site could be resulted from the local resuspension, we reasonably attribute the enhanced SSC events to the identified mesoscale eddy activities utilizing the full-water column records of turbidity and sediment trap systems. The southwest of Taiwan is a typical area for generation of mesoscale eddies and numerous energetic and longlived eddies are born each year and then move southwestward spreading all over of the SCS11. Such eddies are considered to potentially trap and transport tremendous amount of sediments derived from Taiwan or other source areas southwestward and finally release them in the SCS deep basin. Despite of the relatively small amount of the total sediment involved in this study, we consider it an important mechanism for sediment transport in the SCS deep basin that was ignored previously.

This study clarifies that the observed anomalous velocities and enhanced SSC via a full-water column mooring system occurred simultaneously or laggingly with passing-through of the surface mesoscale eddies. The along-slope sediment transport is due to the eddy-driven horizontal advection, depending on the strength and orientation of the geographically and temporally varying SSC. Our study shows that the long-distance sediment transport induced by eddies in the SCS is significant. Considering temporal and spatial variations of the eddies¹¹, there is potential for the cross-basin sediment transport to have the seasonal and interannual variability in the SCS. Our study highlights the significance of surface-generated eddies on the deepwater sedimentary dynamic process and further in general on sedimentary and ecological environments.

Methods

Measurements from the mooring system. A deepwater mooring system (TJ-A-1) was deployed at 2100 m water depth on the northeastern SCS continental slope (117.42°E, 20.05°N) for near two consecutive years from September 2011 to May 2013 (Figure 1a), with a retrieval and redeployment in October 2012. The bathymetry is oriented southeastward. Instruments equipped on the mooring system include 2 sets of sediment traps (McLane MARK 78H-21), a 75 kHz long-ranger Acoustic Doppler Current Profiler (TRDI Workhorse ADCP-LR75), and 2 single-point recording current meters (Aanderaa Seaguard RCM IW). During the first (second) deployment, the downward-looking ADCP-LR75 was placed at 1637 m and sampled velocities every 1 hour (30 min) at a 10-m-bin (5-m-bin) vertical resolution, enabling a measurement ranging from roughly 1655 m to 2015 m. The two sets of RCMs were positioned at 617 m and 2069 m, respectively, recording flow velocity, temperature, turbidity, and dissolved oxygen every 1 hour (20 min). Unfortunately, the turbidity probes failed to function since May 2012 (February 2013) because of the battery shortage. The flux of sediment particulate matters was collected into individual sample bottles of sediment traps, with 15-day and 10-day time series during the two deployments, respectively. However, the lower-layer sediment trap during the first deployment (September 2011 to October 2012) and the upper-layer sediment trap during the second deployment (October 2012 to May 2013) failed in the operation because of mechanical problems. Thus, the comparison of sediments collected only at the lower layer (2068 m) in 2013 (Figure 4c) are

Along-slope and cross-slope current velocities. The raw current velocities obtained from ADCP and RCM are in ENU (East-North-Up) coordinates. In order to be

consistent with the propagating direction of the eddies, the east-west velocity (u_o) and the north-south velocity (v_o) were converted to the along-slope velocity (u_o) northeast-southwest) and cross-slope velocity (v_o) northwest-southeast) as shown in Figure 1b using the following geometrical relationships,

$$u = u_0 \times \cos \theta + v_0 \times \sin \theta$$

$$v \! = \! - u_0 \times \sin\theta \! + \! v_0 \times \cos\theta$$

where $\theta\approx 28^\circ$ is the acute angle between the eddy propagating direction and the ENU coordinates.

Estimate of SSC from turbidity. Selective suspended sediments sampling at the mooring site was implemented to determine the relation between turbidity (FTU) and actual suspended sediment concentration (mg Γ^{-1}) in April 2012 at $\sim\!680$ m and in April 2013 at $\sim\!2000$ m water depth, respectively. The sediments were collected insitu by the large volume water transfer system (WTS-LV04) onto 142 mm membrane filters (4 µm Nuclepore). Using the least square fitting method, a proportional linear relation between the turbidity recorded by RCM and SSC was determined, SSC (mg Γ^{-1}) = 0.96 \times turbidity (FTU). The standard deviation of the error in predicting SSC is 0.01. The filtrated suspended sediment at $\sim\!2000$ m water depth collected in April 2013 was analyzed for clay mineralogy using the X-ray diffraction (XRD) with an analysis precision of 5% 14 . The clay mineral assemblage consists of smectite (35%), illite (35%), chlorite (24%), and kaolinite (6%).

Anomalous velocities. In order to exclude the tides and other signals with higher frequencies than tides from the total current velocities, the subinertial current velocities were computed from ADCP-LR75 and RCM by low-pass filtering via a fourth-order Butterworth filter with a cut-off frequency of 0.33 cycles per day (~72 hours for period), about half of the local inertial frequency *f*. This low-pass filtered velocity was resampled every 24 h to represent daily averaged anomalous velocity that correlates to the passing eddies.

Sea surface data from satellites. A gridded satellite altimetry products of merged sea level anomaly (SLA) and surface geostrophic current velocity distributed by AVISO (Archiving, Validation and Interpretation of Satellite Oceanographic data, http://www.aviso.oceanobs.com) based on TOPEX/Poseidon, Jason-1, ERS-1, and ERS-2 data were used to identify surface mesoscale eddies in the study area. The merged products were downloaded from the global near-real-time (NRT) data files with 1 day interval on a 0.25° resolution at both latitude and longitude. Sea surface temperature (SST) shown in Supplementary Figures S2 and S3 was provided by the Advanced Very High Resolution Radiometer (AVHRR, http://www.ncdc.noaa.gov/sst), with 1 day interval on a 0.25° resolution at both latitude and longitude.

Determination of surface eddies. Cyclonic and anticyclonic eddies are represented by negative and positive SLA in the north hemisphere, respectively. The horizontal scale of the anticyclonic (cyclonic) eddy is determined by the SLA with values of larger (less) than 25 (-25) cm.

Estimate of sediment transport. The near-bottom sediment transport driven by the southwestward-propagating eddies was calculated with the following equation,

$$Transport = SSC \times \mathbf{u} \times A$$

where SSC is the suspended sediment concentration observed near the bottom, \boldsymbol{u} is the observed near-bottom anomalous current velocity vector, and \boldsymbol{A} is the area with the high SSC. In our calculation, \boldsymbol{u} is the depth-mean current velocity about 100 m above the turbidity probe. Due to the absence of spatial measurements on SSC, \boldsymbol{A} is conservatively assumed the area near the bottom boundary with a width of 100 km and a thickness of 100 m^{9,11}. The total sediment transport was computed by integrating the result over time interval when the eddy passed by the mooring site. Specifically, the integrating time period for the first eddy is from 1 February to 10 March 2012, and for the second eddy the integrating time period consists of two enhanced SSC intervals: from 19 to 25 January 2013 and from 30 January to 12 February 2013.

- Lagerloef, G. S. E. The Point Arena Eddy: A recurring summer anticyclone in the California Current. J. Geophys. Res. 97, 12,557–12,568 (1992).
- Liang, X. & Thurnherr, A. M. Eddy-modulated internal waves and mixing on a midocean ridge. J. Phys. Oceanogr. 42, 1242–1248 (2012).
- Dong, C., McWillianms, J. C., Liu, Y. & Chen, D. Global heat and salt transports by eddy movement. Nat. Commun. 5:3294, doi: 0.1038/ncomms4294 (2014).
- Chelton, D. B., Gaube, P., Schlax, M. G., Early, J. J. & Samelson, R. M. The influence of nonlinear mesoscale eddies on near-surface oceanic chlorophyll. *Science* 334, 328–332 (2011).
- 5. Mahadevan, A. Eddy effects on biogeochemistry. *Nature* **506**, 168–169 (2014).
- Gruber, N. et al. Eddy-induced reduction of biological production in eastern boundary upwelling systems. Nat. Geosci. 4, 787–792 (2011).
- 7. Castelao, R. M. & He, R. Mesoscale eddies in the South Atlantic Bight. *J. Geophys. Res. Oceans* 118, 5720–5731 (2013).



- 8. Adams, D. K. et al. Surface-generated mesoscale eddies transport deep-sea products from hydrothermal vents. Science 332, 580-583 (2011).
- Washburn, L., Swenson, M., Largier, J., Kosro, P. & Ramp S. Cross-shelf sediment transport by an anticyclonic eddy off northern California. Science 261, 1560-1564
- 10. Chow, C.-H., Hu, J.-H., Centurioni, L. R. & Niiler, P. P. Mesoscale Dongsha cyclonic eddy in the northern South China Sea by drifter and satellite observations. J. Geophys. Res. 113, C04018, doi: 10.1029/2007JC004542 (2008).
- 11. Xiu, P., Chai, F., Shi, L., Xue, H. & Chao Y. A census of eddy activities in the South China Sea during 1993-2007. J. Geophys. Res. 115, C03012, doi:10.1029/ 2009JC005657 (2010).
- 12. Zhang, Z., Zhao, W., Tian, J. & Liang, X. A mesoscale eddy pair southwest of Taiwan and its influence on deep circulation. J. Geophys. Res. Oceans 118, doi:10.1002/2013JC008994 (2013).
- 13. Becker, J. J. et al. Global bathymetry and elevation data at 30 arc seconds resolution: SRTM30_PLUS. Mar. Geod. 32, 355-371 (2009).
- 14. Liu, Z. et al. Clay mineral distribution in surface sediments of the northeastern South China Sea and surrounding fluvial drainage basins: Source and transport. Mar. Geol. 277, 48-60 (2010).
- 15. Adams, D. K. & Flierl, G. R. Modeled interactions of mesoscale eddies with the East Pacific Rise: Implications for larval dispersal. Deep-Sea Res. I 57, 1163-1176
- 16. Chelton, D. B., Schlax, M. G., Samelson, R. M. & de Szoeke, R. A. Global observations of large oceanic eddies. Geophys. Res. Lett. 34, L15606, doi:10.1029/ 2007GL030812 (2007)
- 17. Chelton, D., Schlax, M. & Samelson, R. Global observations of nonlinear mesoscale eddies. Prog. Oceanogr. 91, 167-216 (2011).
- 18. Kao, S. J., Shiah, F. K., Wang, C. H. & Liu, K. K. Efficient trapping of organic carbon in sediments on the continental margin with high fluvial sediment input off southwestern Taiwan. Cont. Shelf Res. 26, 2520-2537 (2006).
- 19. Liu, Z. et al. Detrital fine-grained sediment contribution from Taiwan to the northern South China Sea and its relation to regional ocean circulation. Mar. Geol. 255, 149-155 (2008).
- 20. Kao, S. J., Jan, S., Hsu, S. C., Lee, T. Y. & Dai, M. Sediment budget in the Taiwan Strait with high fluvial sediment inputs from mountainous rivers: New observations and synthesis. Terr. Atmos. Ocean. Sci. 19, 525-546 (2008).
- 21. Liu, Z. & Stattegger, K. South China Sea fluvial sediments: An introduction. J Asian Earth Sci. 79, 507-508 (2014).

22. Qu, T., Girton, J. B. & Whitehead, J. A. Deepwater overflow through Luzon Strait. J. Geophys. Res. 111, C01002, doi:10.1029/2005JC003139 (2006).

Acknowledgments

Satellite altimetry products distributed by AVISO (http://www.aviso.oceanobs.com) and software Matlab R2010b are greatly appreciated for the use to generate the sea level anomaly map. We thank Shaohua Zhao, Xiajing Li, Quan Chen, Qin Zhang, and Yanli Li for their mooring deployment cruise assistance, and Ke Wen for collecting satellite data. This work is supported by the National Natural Science Foundation of China (91128206, 40925008, and 41106013).

Author contributions

Y.W.Z. analyzed the data and wrote the manuscript. Z.F.L. initiated the idea, designed the study, and contributed to the writing. Y.L.Z. and J.R.L. contributed to the design of the study and the data analysis. W.G.W. contributed to the data analysis. J.P.X. contributed to the design of the study and data discussion.

Additional information

Supplementary information accompanies this paper at http://www.nature.com/ scientificreports

Competing financial interests: The authors declare no competing financial interests.

How to cite this article: Zhang, Y. et al. Mesoscale eddies transport deep-sea sediments. Sci. Rep. 4, 5937; DOI:10.1038/srep05937 (2014).



This work is licensed under a Creative Commons Attribution-NonCommercial NoDerivs 4.0 International License. The images or other third party material in this article are included in the article's Creative Commons license, unless indicated otherwise in the credit line: if the material is not included under the Creative Commons license, users will need to obtain permission from the license holder in order to reproduce the material. To view a copy of this license, visit http:// creativecommons.org/licenses/by-nc-nd/4.0/